Fluctuation phenomena in chaotic Dirac quantum dots: Artificial atoms on graphene flakes

J. G. G. S. Ramos,[1] M. S. Hussein,[2] and A. L. R. Barbosa[3]

[1]*Departamento de Física, Universidade Federal da Paraíba, 58051-970, João Pessoa, Paraíba, Brazil*

[2]*Instituto de Estudos Avançados and Instituto de Física, Universidade de São Paulo, C.P. 66318, 05314-970 São Paulo, SP, Brazil and Departamento de Física, Instituto Tecnológico de Aeronáutica, CTA, São José dos Campos, S.P., Brazil*

[3]*Departamento de Física, Universidade Federal Rural de Pernambuco, Dois Irmãos, 52171-900 Recife, Pernambuco, Brazil*

(Received 8 September 2015; revised manuscript received 29 February 2016; published 21 March 2016)

We develop the stub model for the Dirac quantum dot, an electron confining device on a grapheme surface. Analytical results for the average conductance and the correlation functions are obtained and found in agreement with those found previously using semiclassical calculation. Comparison with available data is presented. The results reported here demonstrate the applicability of random matrix theory in the case of Dirac electrons confined in a stadium.

DOI: 10.1103/PhysRevB.93.125136

I. INTRODUCTION

The electronic transport across a wide class of recently controlled materials displays relativistic properties, although at a speed much slower than light. These structures are known as Dirac materials [1–9] and give rise to intriguing physical phenomena of interest both experimentally and theoretically [10–15]. Quite interesting phenomena emerge from the nature of wave functions of the confined electrons, described by the massless or massive Dirac equation of relativistic quantum mechanics [5,9,16–22], instead of the Schrödinger equation.

The Dirac equation is appropriate to describe the electronic states of two independent sub-lattice components [5,23], which generate additional constraints known as pseudospins. The prominent examples of these bipartite systems are square lattices, such as some topological insulators, and hexagonal lattices, whose main example are the graphene structures.

Among the different electronic Dirac devices, the chaotic Dirac quantum dot (DQD), also called chaotic Dirac billiard (DB), has received a significant highlight [4,18,24–33], due to its universal characteristics. In the search for such universal properties, Ref. [4] studied experimentally a DB using a graphene quantum dot. The authors study a small billiard and show level statistics distribution best described by Gaussian unitary or orthogonal ensembles from the random matrix theory (RMT). Moreover, the authors find evidences of a time-reversal symmetry (TRS) broken state in the absence of a magnetic field, raising questions about the possible origin of such states. In fact, almost 30 years ago, Berry and Mondragon [34] studied what they called "Neutrino Billiard," a stadium where massless spin-1/2 fermions, described by a Dirac Hamiltonian, are confined. They showed that the system exhibits time-reversal symmetry (TRS) breaking in the absence of an external magnetic field. This TRS breaking is of course not the physical one associated with the presence of an external magnetic field. It arises in the above reference as a fictitious single-valley time-reversal symmetry due to the use of the Weyl equation, that is, not the time-reversal symmetry of graphene which is governed by the Dirac equation. The statistics of the energy eigenvalues of the confined fermions in Ref. [34], were found to be governed by the Gaussian unitary ensemble (GUE). Motivated by this and other findings, Ref. [18] uses the tight-binding Dirac Hamiltonian model for electrons, taking into account massive confinement, to analyze the conductance and energy level statistics of graphene DB. In the absence of massive confinement, the authors show that electronic properties are well described by Gaussian unitary or orthogonal ensembles, as obtained in Ref. [4]. However, in the presence of massive confinement, the transmission statistics follow exclusively from the block unitary structure, while the spectral statistics exhibits an orthogonal or even Poisson statistics.

Analytical results for the chaotic graphene quantum dot (with massive confinement were obtained using semiclassical theory in Ref. [24]. In the limit of high massive confinement, the authors predict the average of conductance and the amplitude of the universal fluctuations as a function of magnetic flux and armchair edges. The authors also analyze how the ratio between dwell time and the magnetic flux time ($T_{\rm dwell}/T_B$) as well as dwell time and armchair edges time ($T_{\rm dwell}/T_{\rm ac}$) affect the weak localization and universal fluctuations in the crossover regime and compare with standard results of the Gaussian unitary and orthogonal universal ensembles. Motivated by that semiclassical theory analysis, Ref. [27] performs a full analytical study of the DQD through the RMT chiral ensemble. The authors derived a general expression for the average conductance and its universal fluctuations for the three classes of chiral ensembles in the pure regime (in the absence of crossover fields), which in the semiclassical limit (large number of open channels) recovers the specific results of Ref. [24] that are outside the crossover regime.

As previously discussed, there is a theoretical challenge to construct an RMT formulation for the study of the DQD in any crossover regime (finite field and/or boundary condition). In order to solve the problem, we deduce in this work a generalization of the crossover scattering framework, based on a diagrammatic method which was proposed in Ref. [35], to study the crossover regime in the chaotic Dirac billiard connected to a source and a drain of the conductance electrons. As a relevant application of our framework, we study the chaotic graphene quantum dot (chaotic DQD), obtaining general analytical expressions for the average of the conductance and for the correlation functions of conductance as a function of energy, magnetic flux, straining of the graphene monolayer [10,17], and confinement by massive, armchair and zigzag edges [5,36]. In particular, we show the full suppression of

the weak localization term as a function of the straining, in full agreement with the experimental findings of Ref. [10]. Moreover, in the limit of high massive confinement, we recover the results obtained in Ref. [24] which uses semiclassical theory. However, we emphasize the generality of our RMT framework, which is applicable to all categories of chaotic DQD.

The paper is organized as follows: In Sec. II we give a brief account of the quantum chaotic scattering theory employed in the RMT treatment of the chaotic Dirac quantum dot (CDQD). In Sec. III, we introduce the RMT crossover scattering framework to the chaotic Dirac billiard. In Sec. IV, we include a brief discussion of the effective graphene Hamiltonian and apply it to discuss the statistical properties of the CDQD. We perform calculations and obtain general analytical expressions for the average of conductance and its correlation functions and also analyze their relevant limits. The conclusions are given in Sec. V.

II. QUANTUM CHAOTIC SCATTERING THEORY AND THE RMT-BASED STUB MODEL

In a general stadium which confines electrons one can describe the conductance and its universal fluctuations using known methods of resonant scattering. The electrons inside the stadium execute confining potential-affected motion governed by the Schrödinger or the Dirac equation. The electrons suffer multiple reflections from the boundaries and standing waves are generated, which represent the eigenstates of the system. Taking into account the coupling of the interior of the stadium to the outside region results in transforming the standing waves into resonances with a width that measures the time it takes the electrons to be transmitted to the outside and electric conductance ensues. A convenient way to formalize the above, is through Feshbach's projection operator method, commonly used to treat the compound nucleus resonances in nuclear reactions [37–40]. Denoting the total wave function of the system by $|\Psi\rangle$, one introduces the projector Q which projects out the closed channels, namely the states in the interior of the stadium. The states with electrons outside the stadium, namely the open channels are projected out by P, with $PQ = QP = 0$ and $P^2 = P$, and $Q^2 = Q$. The wave equation of the whole many-electron system, can then be decomposed into two coupled equations, one for $P|\Psi\rangle$ and the other for $Q|\Psi\rangle$. The exact, full Hamiltonian of the system H, is also decomposed into four operators, viz $QHQ + PHP + PHQ + QHP$. After well-known manipulations one is able to derive a general exact expression for the scattering matrix S, that describes resonant scattering,

$$S = 1 - 2i\pi PHQ \frac{1}{E - QHQ - QHP\frac{1}{E-PHP+i\varepsilon}PHQ} \times QHP. \quad (1)$$

Writing $QHP[1/(E - PHP + i\varepsilon)]PHQ = -i\pi QHP\delta(E - PHP)PHQ + QHPPr[1/(E - PHP)]PHQ \equiv -i\Gamma_Q/2 + \Delta_Q$, where Γ_Q is the width operator of the resonances, and Δ_Q is the real energy shift operator which is usually added to QHQ to define the resonance Hamiltonian. Thus,

$$S = 1 - 2i\pi PHQ \frac{1}{E - [QHQ + \Delta_Q] + i\frac{\Gamma_Q}{2}} QHP. \quad (2)$$

The above expression of the S matrix is exact. For application to a given physical system, one has to specify the Hamiltonian QHQ of the isolated closed stadium or quantum dot, and use a spectral decomposition of $\delta(E - PHP)$. This is accomplished in [41], and used extensively by [42]. Neglecting the energy shift operator, and using matrix notation, the S matrix which constitutes the basic theoretical object in quantum chaotic scattering theory based on RMT is

$$S = 1 - 2i\pi W^T \frac{1}{E - H + i\pi WW^T} W, \quad (3)$$

where W is a real nonrandom matrix that represents the coupling of the internal region with the open channels, and H is taken as a random Hamiltonian pertaining to one of the university classes of random matrices, the Gaussian orthogonal ensemble (GOE) with TRI, the Gaussian unitary ensemble, with TRI breaking, and the Gaussian symplectic ensemble (GSE). When using one of these ensembles to calculate averages of $SS^\dagger$ or $SSS^\dagger S^\dagger$, the distribution $P(H)$ is required. Analytical evaluation of these averages is quite involved as they require the evaluation of complicated triple integrals. Only in the case of GUE was it possible to actually obtain closed form expressions [42]. Generally, researchers rely on numerical simulations using the random matrix generator [43]. Application of this theory to to microwave resonator physics is an ongoing program [44].

An alternative method which allows the obtention of analytical results for any of the ensembles is based on the distribution of the S matrix itself, $P(S)$ [45]. The ensemble here is Dyson's circular unitary ensemble (CUE). The stub model is based on this approach (see [46]), and it amounts to attaching a stub (fictitious) to the quantum dot and using it as a scaffolding to build the S matrix. The size of the stub is chosen so that the dwell time in it is much larger than the dwell time in the dot. Further, the permanence time of the electrons inside the dot + stub system τ_p is much shorter than the escape time $\tau_{\rm esc}$ to the leads and open channels. These conditions guarantee that all the variables in the system, the Fermi energy ε, and the magnetic field B, are made to be explicitly present in the reflection matrix R [of dimension $(M - N)$] of the stub, leaving the S matrix of the dot (without the stub), U, of dimension $M \times M$, be a product of 2×2 spin matrix times a matrix at $\varepsilon = 0$, $B = 0$, and zero spin-orbit scattering rate. As such the dot S-matrix U can be chosen from Dyson's circular orthogonal ensemble of random matrix theory. It has been shown [46] that the S matrix of the system (dot plus leads) is

$$S = PU(1 - Q^\dagger RQU)^{-1}P^\dagger, \quad (4)$$

where P and Q are projection matrices of dimensions, $N \times M$ and $(M - N) \times M$, respectively. It has been proven that owing to the second condition on the time scales, namely, $\tau_p \ll \tau_{\rm esc}$, the S matrix above remains unaffected by the stub and in fact equivalent to the Hamiltonian-based S matrix [Eq. (3)] [47,48]. Thus the characterization of the stub as a scaffolding is appropriate. To perform averages of S, one expands in

powers of U and uses diagrammatic techniques as developed by [47,48].

We turn now to a Dirac version of the S-matrix distribution approach and the stub model.

III. CROSSOVER SCATTERING FRAMEWORK FOR THE GENERAL DIRAC BILLIARD

In this section, to study the crossover regime in the chaotic Dirac billiard connected to leads, we introduce a generalization of the crossover scattering framework, which was proposed in Ref. [35]. We begin by employing quantum chaotic scattering theory, and introduce the stub model discussed in the previous section for the chaotic Schrödinger quantum dot. Within the stub model the scattering matrix as a function of external parameters such as the energy ϵ and magnetic flux $\mathcal{B}$, and an an internal parameter which is the massive mass term m in the generic Dirac Hamiltonian, is given by

$$\mathcal{S}(\epsilon,\mathcal{B},m) = \mathcal{P}[\mathbb{1} - \mathcal{Q}^{\dagger}\mathcal{R}(\epsilon,\mathcal{B},m)\mathcal{Q}\mathcal{U}]^{-1}\mathcal{U}\mathcal{P}^{\dagger}. \tag{5}$$

The matrices $\mathcal{S}(\epsilon,\mathcal{B},m)$ and $\mathcal{U}$ have dimension $N_T \times N_T$ and $M \times M$, respectively. The total number of open channels $N_T = N_1 + N_2$ is the sum of open channels in the leads 1 and 2, while M is the number of resonances in the chaotic Dirac quantum dot. The matrix $\mathcal{U}$ can be a member of the circular orthogonal ensemble instead of chiral orthogonal ensemble if we assume $N_T \gg 1$. In this limit, Chiral universality classes give the same results of Wigner-Dyson universality classes as proved in Ref. [27]. The matrices $\mathcal{P}$ and $\mathcal{Q}$ are the projector operators of order $N_T \times M$ and $(M - N_T) \times M$, respectively, with elements given by $\mathcal{Q}_{ij} = \delta_{i+N_T,j}$ and $\mathcal{P}_{ij} = \delta_{ij}$. We intend to incorporate additional degrees of freedom on the formalism, two for each subspace, with the prominent example the structure of the graphene Hamiltonian. Accordingly, the elements of the matrices $\mathcal{U}$, $\mathcal{P}$, and $\mathcal{Q}$ are all proportional to the $\sigma_0 \otimes \tau_0$, with σ_0 and τ_0 denoting 2×2 identity matrices. The matrix $\mathcal{R}(\epsilon,\mathcal{B},m)$ has dimension $(M - N_T) \times (M - N_T)$ and is parametrized as

$$\mathcal{R}(\epsilon,\mathcal{B},m) = \exp\left\{\frac{i}{M}\left[2\pi\frac{\epsilon}{\Delta}\sigma_0 \otimes \tau_0 - \mathcal{H}(\mathcal{B},m)\right]\right\}. \tag{6}$$

In Eq. (6), the universal Hamiltonian $\mathcal{H}(\mathcal{B},m)$ is obtained from the effective Dirac Hamiltonian preserving its intrinsic symmetries and considering its amplitudes as members of a Gaussian distribution. We consider the additional degrees of freedom residing in the elements of matrices $\mathcal{H}(\mathcal{B},m)$ which are all proportional to $\sigma_i \otimes \tau_j$, with σ_i and τ_j denoting Pauli matrices $(i,j = x,y,z)$ in each subspace of the Dirac Hamiltonian.

The conductance of the chaotic Dirac quantum dot at zero temperature can be written as a function of the scattering matrix, Eq. (5), as follows:

$$\frac{G}{e^2/h} = 4 \times \frac{N_1 N_2}{N_T} + \mathrm{Tr}[\mathcal{S}\,\mathcal{K}\,\mathcal{S}^{\dagger}\,\mathcal{K}], \tag{7}$$

where the elements of the matrix $\mathcal{K}$ are $\mathcal{K}_{ii} = N_2/N_T$, $\mathcal{K}_{ii} = -N_1/N_T$ and $\mathcal{K}_{ij} = 0$ for $i = 1,\ldots,N_1, i = N_1+1,\ldots,N_T$, and $i \neq j$, respectively. The factor 4 arises from the degeneracies of the two subspaces represented by σ and τ. The average of the conductance, Eq. (7), can be obtained using the relation,

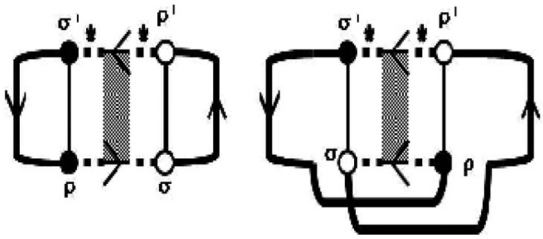

FIG. 1. Diffuson (left) and cooperon (right) diagrams for the average of conductance [Eq. (7)].

$$\langle \mathcal{S}_{ij;\alpha\beta;\rho\delta}(\epsilon,\mathcal{B},m)\mathcal{S}^{*}_{i'j';\alpha'\beta';\rho'\delta'}(\epsilon',\mathcal{B},m)\rangle = \delta_{ii'}\delta_{jj'}\mathcal{D}_{\alpha\beta,\rho\delta;\beta'\alpha',\delta'\rho'} + \delta_{ij'}\delta_{ji'}(\mathcal{T}\mathcal{C}\mathcal{T})_{\alpha\beta,\rho\delta;\beta'\alpha',\rho'\delta'}, \tag{8}$$

whose validity is over the limit $M \gg N_T \gg 1$. The $\mathcal{T}$ carries symmetries as the time reversal of the Dirac Hamiltonian and is defined as $\mathcal{T} = \sigma_0 \otimes \tau_0 \otimes \mathcal{T}_{\chi}$. The indices $\alpha,\beta = 1,2$ are associated with the subspace σ, while $\rho,\delta = 1,2$ with the subspace τ. The matrices $\mathcal{D}$ and $\mathcal{C}$ are contributions of diffuson and cooperon diagrams, which are represented in Fig. 1, and obtained by following expressions

$$\begin{aligned}\mathcal{D}^{-1} &= M\sigma_0 \otimes \tau_0 \otimes \sigma_0 \otimes \tau_0 - \mathrm{Tr}(\mathcal{R} \otimes \mathcal{R}^{\dagger}),\\ \mathcal{C}^{-1} &= M\sigma_0 \otimes \tau_0 \otimes \sigma_0 \otimes \tau_0 - \mathrm{Tr}(\mathcal{R} \otimes \mathcal{R}^{\star}),\end{aligned} \tag{9}$$

where $\dagger$ designates Hermitian conjugation and $\star$, complex conjugation. From Eqs. (7) and (8), we can obtain the following expression for the average conductance:

$$\frac{\langle G\rangle}{e^2/h} = 4 \times \frac{N_1 N_2}{N_T} - \frac{N_1 N_2}{N_T}\sum_{\rho,\delta}[\mathrm{Tr}(\mathcal{T}\mathcal{C}\mathcal{T})]_{\rho\sigma;\rho\delta}, \tag{10}$$

where the trace involves the two subspaces using the following general cross product:

$$[\mathrm{Tr}(\sigma_i \otimes \tau_j \otimes \sigma_k \otimes \tau_l)]_{\rho\delta;\rho'\delta'} = \left[\left(\sum_{\alpha\beta}(\sigma_i)_{\alpha\beta}(\sigma_k)_{\beta\alpha}\right)\tau_j \otimes \tau_l\right]'_{\rho\delta,\rho'\delta'}.$$

The calculation algebra of Eq. (10) is performed using the backward multiplication as follows:

$$\begin{aligned}&(\sigma_i \otimes \tau_j \otimes \sigma_k \otimes \tau_l)\cdot(\sigma_{i'} \otimes \tau_{j'} \otimes \sigma_{k'} \otimes \tau_{l'})\\ &= (\sigma_i\sigma_{i'}) \otimes (\tau_{j'}\tau_j) \otimes (\sigma_{k'}\sigma_k) \otimes (\tau_l\tau_{l'}).\end{aligned}$$

The same algebraic analysis can be applied to the covariance of conductance. We perform the calculation and, after some algebra, we obtain the following expression:

$$\frac{\mathrm{cov}[G(\epsilon,\mathcal{B}),G(\epsilon',\mathcal{B}']}{e^4/h^2} = \frac{N_1^2 N_2^2}{N_T^2}[\mathcal{V}_{\mathcal{D}} + \mathcal{V}_{\mathcal{C}}], \tag{11}$$

where

$$\mathcal{V}_{\mathcal{D}} = \sum_{\rho,\sigma}[\mathrm{Tr}\mathcal{D}]_{\rho\sigma;\rho'\sigma'}[\mathrm{Tr}\mathcal{D}]_{\sigma'\rho';\sigma\rho},$$

$$\mathcal{V}_{\mathcal{C}} = \sum_{\rho,\sigma}[\mathrm{Tr}(\mathcal{T}\mathcal{C}\mathcal{T})]_{\rho\sigma;\rho'\sigma'}[\mathrm{Tr}(\mathcal{T}\mathcal{C}\mathcal{T})]_{\rho'\sigma';\rho\sigma}.$$

To finalize this section, we can conclude that the crossover scattering model presented above is general and applicable to any kind of chaotic Dirac quantum dot in the ballistic regime. It is important to point out here as shown by Ref. [49], that classical consideration of impurities can be incorporated through a semiclassical S matrix of the Miller type which contains a Maslov index. In our formulation, we can, in principle, introduce a term of this type and study its consequence on our results. We find this a very interesting line of research and hope to carry out the development in the future. This will allow us to study the diffusive regime. As already stated our present approach only allows us to study the ballistic regime. We need only to get the matrix $\mathcal{H}(\mathcal{B},m)$ from the Dirac Hamiltonian together with Eqs. (6) and (9)–(11) to obtain the averages of conductance and covariance. In the next section, we will apply the framework in the relevant example of a chaotic graphene quantum dot. We will present general results and, at specific limits, we recover the results of Ref. [24].

IV. CHAOTIC GRAPHENE QUANTUM DOT

In this section, we apply the crossover scattering model, which was described in the previous section, to study a general chaotic graphene quantum dot. First, the effective Hamiltonian of graphene is presented together with the symmetries of the problem. Following this, the characteristic and general effective graphene matrix $\mathcal{H}(\mathcal{B},m)$ is introduced and used in the calculation of the average of conductance and covariance, Eqs. (10) and (11), respectively.

In fact the Hamiltonian describing the graphene was obtained for energies (Dirac) close to the Fermi energy. Having in mind the homogeneity of the spectrum, we have fixed the Ferm energy to be zero. Close to the Dirac point there exist many energy levels available for the massive Hamiltonian used by us. The size of the quantum dot is determined by the presence of about 10^5 carbon atoms (size of the lattice is about 10^3 a, where the lattice constant $a = 0.25$ nm).The lattice is hexagonal and the confining terms are generated by smooth and quasilocalized interactions at the edges, determined by the zig-zag or arm-chair symmetry. In this case the quantum dot, in the universal regime, could furnish about 10^3 energy levels close to the Dirac point, as was observed through numerical simulations by Ref. [18]. The other terms in the Hamiltonian are also of short range in nature with the Dirac point centered at the edge of the energy spectrum (Fermi energy) and all produce results in the universal regime.

A. Effective Hamiltonian of graphene

Following [5,18,36], the effective Hamiltonian of graphene for low energies and long length scales without spin degree freedom can be written as

$$\mathcal{H}_{\rm eff} = v[\mathbf{p} - e\mathbf{A}\cdot\sigma]\otimes\tau_0 + ev[A(\mathbf{r})\cdot\sigma]\otimes\tau_z + w_{ac}(\mathbf{r})\sigma_z\otimes\tau_y + m(\mathbf{r})\sigma_z\otimes\tau_z + w_{zz}(\mathbf{r})\sigma_z\otimes\tau_z, \quad (12)$$

where the Pauli matrices σ_i and τ_i act on the sublattice and valley degrees of freedom, respectively. The vector potential $\mathbf{A}$ carries information about the external electromagnetic fields, and has no role in coupling the two valleys. The two valleys are coupled by a valley-dependent vector potential $A(\mathbf{r})$ produced by straining the monolayer [10,17]. The boundary of the chaotic graphene quantum dot is described by three physically relevant boundary types, which are known as confinement by the mass term ($m(\mathbf{r})$), confinement by the armchair edges term ($w_{ac}(\mathbf{r})$), and confinement by the zigzag edges term. However, there are four antiunitary symmetries operating in graphene: $\mathcal{T}_\chi = \sigma_y\otimes\tau_\chi C$ with $\chi = \{0,x,y,z\}$, with C the operator of complex conjugation. $\mathcal{T}_y$ is the time-reversal operation that interchanges the valleys, while $\mathcal{T}_x$ is the valley symmetry. $\mathcal{T}_0$ is called a symplectic symmetry, does not interchange the valleys, and is broken by massive term and valley-dependent vector potential.

B. Average of conductance

The central feature responsible for the simplified random-matrix description of the crossover in the universal regime is the fact that all relevant time scales are much longer than the electron transit time $T_{\rm erg}$, thus $T_{\mathcal{B}}, T_{st}, T_{ac}, T_m, T_{zz} \gg T_{\rm erg}$. In fact, for a very small grapheme flake and in the transition from classical to quantum regimes, the trajectories can be influenced in different manners by the presence of the magnetic field [50]. In the universal regime, however, when many energy levels are available (10^3), all phase space is explored with no preference to some specific trajectories, as long as the dwell time $T_{\rm dwell}$ is greater than the ergodic time $T_{\rm erg}$. In our approach described in the current paper, in the universal regime, $T_{\rm dwell} \gg T_{\rm erg}$, our results are not affected by special trajectories.

The relevance of the crossover effect is guaranteed by the requirement that T's are of the order of the inverse mean level spacing in the chaotic graphene quantum dot [also called chaotic Dirac quantum dot (CDQD)]. We may thus introduce the following dimensionless parameters to characterize the intensity of symmetry breaking in the system:

$$x^2 = \frac{2\pi\hbar}{\Delta T_{\mathcal{B}}},\quad w_{st}^2 = \frac{2\pi\hbar}{\Delta T_{st}},$$
$$w_{ac}^2 = \frac{2\pi\hbar}{\Delta T_{ac}},\quad m^2 = \frac{2\pi\hbar}{\Delta T_m},\quad w_{zz}^2 = \frac{2\pi\hbar}{\Delta T_{zz}},$$

where Δ is the mean level spacing. From Eq. (12), the random-matrix models for the effective Hamiltonians of graphene then follow directly from general symmetry considerations. They are given by

$$\mathcal{H} = ix\ A_1\ \sigma_x\otimes\tau_0 + ix\ A_2\ \sigma_y\otimes\tau_0 + iw_{st}\ B_1\ \sigma_x\otimes\tau_z + iw_{st}\ B_2\ \sigma_y\otimes\tau_z + iw_{ac}\ Y\ \sigma_z\otimes\tau_y + imX\ \sigma_z\otimes\tau_z + iw_{zz}\ Z\ \sigma_z\otimes\tau_z, \quad (13)$$

where the matrices A_i, B_i, X, Y e Z are real antisymmetric with $\langle{\rm Tr}(A_i A_j^T)\rangle = \langle{\rm Tr}(B_i B_j^T)\rangle = \delta_{ij}M^2$ e $\langle{\rm Tr}(XX^T)\rangle = \langle{\rm Tr}(YY^T)\rangle = \langle{\rm Tr}(ZZ^T)\rangle = M^2$.

Now, we can substitute Eq. (13) in Eqs. (6) and (9) and after some algebraic manipulations, we obtain

$$\mathcal{D}^{-1} = \mathcal{C}^{-1} = \mathcal{N}\ (\sigma_0\otimes\tau_0\otimes\sigma_0\otimes\tau_0) - x\ x'(\sigma_x\otimes\tau_0\otimes\sigma_x\otimes\tau_0 + \sigma_y\otimes\tau_0\otimes\sigma_y\otimes\tau_0) - w_{st}^2(\sigma_x\otimes\tau_z\otimes\sigma_x\otimes\tau_z + \sigma_y\otimes\tau_z\otimes\sigma_y\otimes\tau_z) - w_{ac}^2\ (\sigma_z\otimes\tau_y\otimes\sigma_z\otimes\tau_y) - \left(m^2 + w_{zz}^2\right)(\sigma_z\otimes\tau_z\otimes\sigma_z\otimes\tau_z), \quad (14)$$

where $\mathcal{N} = N_T - 2\pi i(\epsilon - \epsilon') + x^2 + x'^2 + 2w_{st}^2 + w_{ac}^2 + m^2 + w_{zz}^2$. Taking the inverse in Eq. (14) we can calculate the average of the conductance from Eq. (10), with $\mathcal{T} = \sigma_0 \otimes \tau_0 \otimes \sigma_y \otimes \tau_0$, and we find the following general expression:

$$\frac{\langle G\rangle}{e^2/h} = 4 \times \frac{N_1 N_2}{N_T} - 2 \times \frac{N_1 N_2}{N_T} \times \left[\frac{1}{N_C + 2w_{st}^2} + \frac{1}{N_C + 2w_{st}^2 + 2m^2 + 2w_{zz}^2} + \frac{1}{N_C + 2w_{st}^2 + 2w_{ac}^2 + 2m^2 + 2w_{zz}^2} - \frac{1}{N_C + 2w_{st}^2 + 2w_{ac}^2} \right], \tag{15}$$

where $N_C = N_T + 2x^2$ with $\epsilon = \epsilon'$ and $x = x'$. Equation (15) is the first major result of our work. The first term expresses Ohm's Law, while the remaining ones are known as the weak localization part of the average $\langle G_{\rm wl}\rangle$.

Let us analyze some relevant limits of Eq. (15). As expected, the limit $x \to \infty$ leads to $\langle G_{\rm wl}\rangle \to 0$. A simple expression can be obtained by taking $m = w_{zz} = 0$ in Eq. (15):

$$\frac{\langle G_{\rm wl}\rangle}{G_0} = -\frac{2}{1 + 2\mathcal{X}^2 + 2\mathcal{W}_{st}^2}, \tag{16}$$

which was obtained through a change of variables, $x^2 = \mathcal{X}^2 N_T$, $b^2 = \mathcal{W}_{st}^2 N_T$, and $G_0 = e^2/h \times 2 \times N_1 N_2/N_T^2$. From Eq. (16), we can conclude that weak localization is not affected by armchair edge (w_{ac}) if there are nonmassive or zigzag edges present. In the Fig. 2(a) we show Eq. (16) as a function of magnetic flux ($\mathcal{X}$) for the following values of $\mathcal{W}_{st} = 0, 0.5, 1, 3$ (from top to bottom). Without straining ($\mathcal{W}_{st} = 0$), Fig. 2(a) shows a weak localization peak. However, the peak becomes prominent with the increase in straining in monolayer CDQD. This result is in complete agreement with theoretical predictions of Ref. [17] and with the experimental measurement of Ref. [10], which showed absence of a weak localization peak in the monolayer of graphene because of straining [see Fig. 2(a) of [10]].

In order to recover the results of [24], we take the limit $m \to \infty$ in Eq. (15). We obtain

$$\frac{\langle G_{\rm wl}\rangle}{G_0} = -\frac{1}{1 + 2\mathcal{X}^2 + 2\mathcal{W}_{st}^2} + \frac{1}{1 + 2\mathcal{X}^2 + 2\mathcal{W}_{st}^2 + 2\mathcal{W}_{ac}^2}, \tag{17}$$

where $w_{ac}^2 = \mathcal{W}_{ac}^2 N_T$. In the case without straining ($\mathcal{W}_{st} = 0$), Eq. (17) reduces to Eq. (71) of Ref. [24]. In Fig. 2(b) we show Eq. (17) as a function of the magnetic flux ($\mathcal{X}$) through the system for values of $\mathcal{W}_{ac} = 0, 1, \infty$ (from bottom to top) and $\mathcal{W}_{st} = 0$. For $\mathcal{W}_{ac} = 0$ the weak localization peak is absent, while it reaches a maximum for $\mathcal{W}_{ac} \to \infty$.

In the limit $w_{zz} \to \infty$, Eq. (15) reduces to Eq. (17). This is interesting, as massive and zigzag edges are physically different but serve the same purpose as far as weak localization is concerned [see Eq. (15)]. This fact contributes to our conclusion that the armchair edge is only relevant in the presence of massive or zigzag edges.

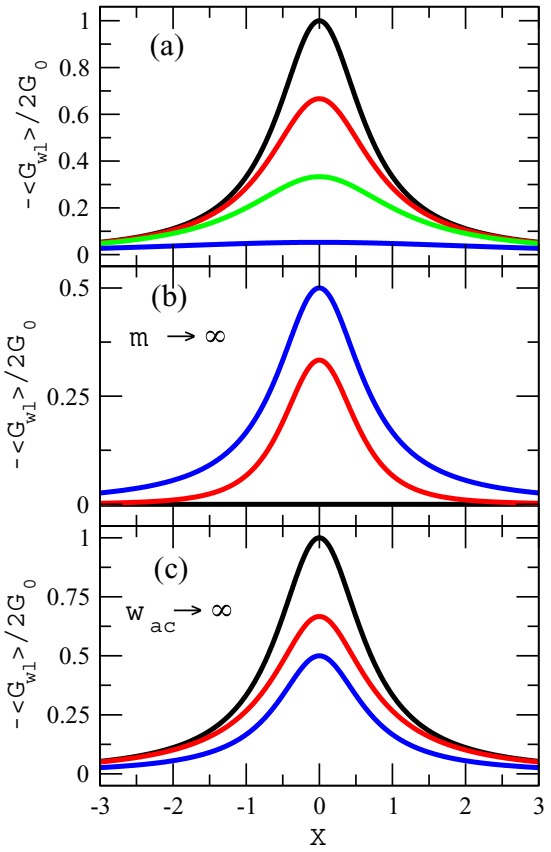

FIG. 2. (a) Equation (16) is plotted as a function of the magnetic flux for $\mathcal{W}_{st} = 0, 0.5, 1, 3$ (from top to bottom). (b) Equation (17) is plotted as a function of the magnetic flux for $\mathcal{W}_{ac} = 0, 1, \infty$ (from bottom to top). (c) Equation (18) is plotted as a function of the magnetic flux for $\mathcal{M} = 0, 1, \infty$ (from top to bottom) and $\mathcal{W}_{zz} = \mathcal{W}_{st} = 0$.

The last important limit can be obtained from Eq. (15) by letting $w_{ac} \to \infty$,

$$\frac{\langle G_{\rm wl}\rangle}{G_0} = -\frac{1}{1 + 2\mathcal{X}^2 + 2\mathcal{W}_{st}^2} - \frac{1}{1 + 2\mathcal{X}^2 + 2\mathcal{W}_{st}^2 + 2\mathcal{M}^2 + 2\mathcal{W}_{zz}^2}, \tag{18}$$

where $m^2 = \mathcal{M}^2 N_T$, $w_{zz}^2 = \mathcal{W}_{zz}^2 N_T$. In Fig. 2(c) we show Eq. (18) as a function of the magnetic flux ($\mathcal{X}$) for $\mathcal{M} = 0, 1, \infty$ (from top to bottom) and $\mathcal{W}_{zz} = \mathcal{W}_{st} = 0$. For $\mathcal{M} \to \infty$ the weak localization peak decreases by a factor of two. The same conclusions are reached by fixing $\mathcal{M} = \mathcal{W}_{st} = 0$ and varying $\mathcal{W}_{zz}$.

C. Covariance of conductance

Here we analyze how the weak localization peak is affected by the magnetic flux and edges. For this purpose we consider the covariance of conductance as a function of energy and magnetic flux using the same method described previously. From Eqs. (11) and (14), we obtain the following general

expression:

$$\frac{\mathrm{cov}[G(\epsilon,x),G(\epsilon',x')]}{e^4/h^2} = 4\times\frac{N_1^2N_2^2}{N_T^2}\times\left[\frac{1}{|N_{\mathcal{D}}|^2}+\frac{1}{\left|N_{\mathcal{D}}+2w_{ac}^2\right|^2}+\frac{1}{\left|N_{\mathcal{D}}+4w_{st}^2+2m^2+2w_{zz}^2\right|^2}\right.$$
$$+\frac{1}{\left|N_{\mathcal{D}}+4w_{st}^2+2m^2+2w_{zz}^2+2w_{ac}^2\right|^2}+\frac{1}{\left|N_{\mathcal{C}}+2w_{st}^2\right|^2}+\frac{1}{\left|N_{\mathcal{C}}+2w_{st}^2+2m^2+2w_{zz}^2\right|^2}$$
$$\left.+\frac{1}{\left|N_{\mathcal{C}}+2w_{st}^2+2w_{ac}^2\right|^2}+\frac{1}{\left|N_{\mathcal{C}}+2w_{st}^2+2m^2+2w_{zz}^2+2w_{ac}^2\right|^2}\right], \tag{19}$$

where $N_{\mathcal{D}} = N_T + 2i\pi(\epsilon-\epsilon')/\Delta + (x-x')^2/2$ e $N_{\mathcal{C}} = N_T + 2i\pi(\epsilon-\epsilon')/\Delta + (x+x')^2/2$. Equation (19) is the second major result of our work. The first four terms of Eq. (19) are diffuson diagram contributions that vanish in the presence of magnetic flux, while the remaining terms are cooperon diagram contributions, which evanesce in the presence of magnetic flux ($x\to\infty$).

Next we analyze the same limits of Eq. (19). Taking $\epsilon=\epsilon'$, $x=x'$, without magnetic flux and setting the others equal to zero, the variance of the conductance from Eq. (19) is given by $\mathrm{var}[G] = G_0^2\times[4\times2]$, where the factor 4 is the degeneracy of the sub-lattice and valley symmetries and the factor 2 comes about from time-reversal symmetry. Further, in the presence of magnetic flux, the variance of the conductance is given by $\mathrm{var}[G] = G_0^2\times[4\times1]$, which indicates that time-reversal symmetry is broken; see top curve of Fig. 3(a).

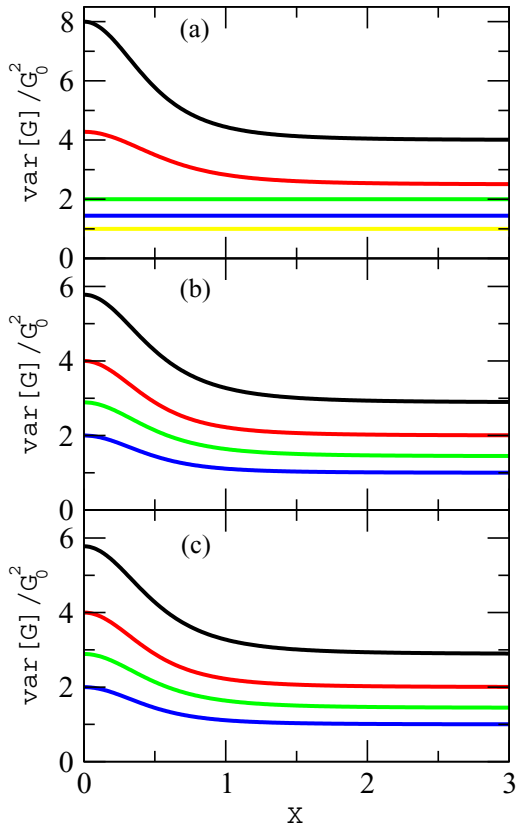

FIG. 3. (a) Equation (19) was plotted (top to down) for $\mathcal{W}_{st} = 0,0.5,\infty$ ($\mathcal{W}_{ac}=\mathcal{W}_{zz}=\mathcal{M}=0$) beyond Eq. (20) for $\mathcal{W}_{ac}=0.5,\infty$. (b) Equation (19) is plotted (top to down) for $\mathcal{M}=0.5,\infty$ ($\mathcal{W}_{st}=\mathcal{W}_{ac}=\mathcal{W}_{zz}=0$) and Eq. (21) for $\mathcal{W}_{ac}=0.5,\infty$ ($\mathcal{W}_{st}=0$). (c) Equation (19) was plotted (top to down) for $\mathcal{W}_{ac}=0.5,\infty$ ($\mathcal{W}_{st}=\mathcal{M}=\mathcal{W}_{zz}=0$) beyond Eq. (22) for $\mathcal{M},\mathcal{W}_{zz}=0.5,\infty$ ($\mathcal{W}_{st}=0$).

Simple expression can been obtained taking $w_{st}\to\infty$ in Eq. (19):

$$\frac{\mathrm{var}[G]}{G_0^2} = \sum_{i=0}^{1}\frac{1}{\left(1+2i\mathcal{W}_{ac}^2\right)^2}. \tag{20}$$

Note that two diffuson and all cooperon contributions have vanished, indicating the breaking time-reverse symmetry. From Eq. (20), only armchair edges are relevant in the presence of straining. Moreover, the average of variances are given by $\mathrm{var}[G] = G_0^2\times[2\times1]$ and $\mathrm{var}[G] = G_0^2\times[1\times1]$ for $\mathcal{W}_{ac}=0$ and $\mathcal{W}_{ac}\to\infty$, respectively. In Fig. 3(a) we show (top to down) Eq. (19) for $\mathcal{W}_{st}=0,0.5,\infty$ ($\mathcal{W}_{ac}=\mathcal{W}_{zz}=\mathcal{M}=0$), and Eq. (20) for $\mathcal{W}_{ac}=0.5,\infty$.

Taking $m\to\infty$(or $w_{zz}\to\infty$) in Eq. (19), four terms go to zero, two diffuson and two cooperon contributions. In this case, Eq. (19) simplifies to

$$\frac{\mathrm{var}[G]}{G_0^2} = \sum_{i,j=0}^{1}\frac{1}{\left(1+2i\mathcal{X}^2+2i\mathcal{W}_{st}^2+2j\mathcal{W}_{ac}^2\right)^2}. \tag{21}$$

In the case without straining ($\mathcal{W}_{st}=0$), Eq. (21) reduces to Eq. (84) of Ref. [24]. Without magnetic flux and setting the other parameters equal to zero, the variance of the conductance from Eq. (21) is given by $\mathrm{var}[G] = G_0^2\times[2\times2]$, which means that the degeneracy factor is reduced by a factor of two and time-reversal symmetry is not broken by the massive edge. Moreover, with magnetic flux on, the variance of the conductance is given by $\mathrm{var}[G] = G_0^2\times[2\times1]$. On the other hand, if $\mathcal{W}_{ac}\to\infty$ and $\mathcal{W}_{st}=0$ the variance from Eq. (21) goes to $\mathrm{var}[G] = G_0^2\times[1\times2]$ and $\mathrm{var}[G] = G_0^2\times[1\times1]$ without and with magnetic flux, respectively. In Fig. 3(b) we show (top to down) Eq. (19) for $\mathcal{M}=0.5,\infty$ ($\mathcal{W}_{st}=\mathcal{W}_{ac}=\mathcal{W}_{zz}=0$) and Eq. (21) for $\mathcal{W}_{ac}=0.5,\infty$ ($\mathcal{W}_{st}=0$).

The last limit we consider, $w_{ac}\to\infty$, in Eq. (19), gives

$$\frac{\mathrm{var}[G]}{G_0^2} = \sum_{i=0}^{1}\frac{1}{\left(1+4i\mathcal{W}_{st}^2+2i\mathcal{M}^2+2i\mathcal{W}_{zz}^2\right)^2}$$
$$+\sum_{i=0}^{1}\frac{1}{\left(1+2\mathcal{X}^2+2\mathcal{W}_{st}^2+2i\mathcal{M}^2+2i\mathcal{W}_{zz}^2\right)^2}. \tag{22}$$

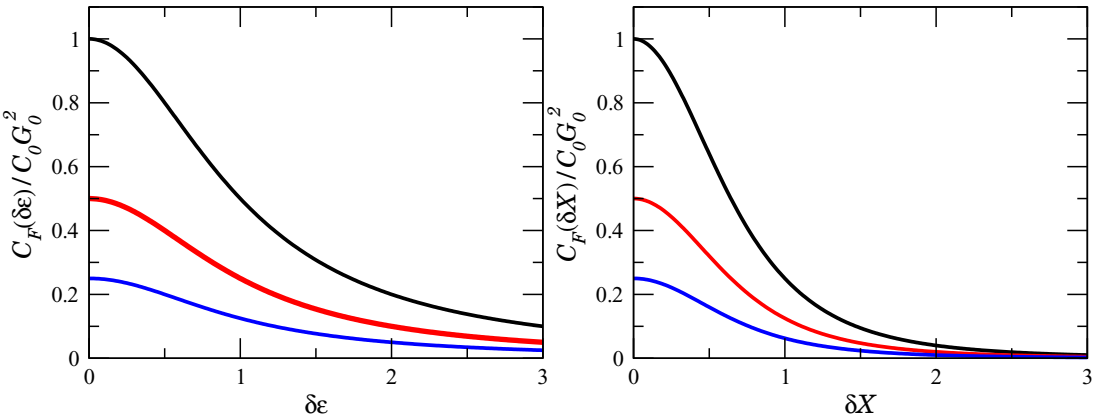

FIG. 4. Typical Lorentzian (left) and quadratic Lorentzian correlation function from Eq. (23) for (top to down) all parameters null, $\{\mathcal{X},\mathcal{M},\mathcal{W}_{ac},\mathcal{W}_{zz}\to\infty\}$ and $\mathcal{W}_{st}\to\infty$.

In this case, the contributions of two diffusons and two cooperons vanish. Fixing $\mathcal{W}_{st}=0$ and turning off the magnetic flux, the variance of Eq. (22) becomes $\mathrm{var}[G]=G_0^2\times[2\times2]$ and $\mathrm{var}[G]=G_0^2\times[1\times2]$ for $\mathcal{M},\mathcal{W}_{zz}=0$ and $\mathcal{M},\mathcal{W}_{ac}\to\infty$, respectively, which indicates that time-reversal symmetry is preserved in both cases. On the other hand, with magnetic flux turned on, the variance of Eq. (22) goes to $\mathrm{var}[G]=G_0^2\times[2\times1]$ and $\mathrm{var}[G]=G_0^2\times[1\times1]$ for $\mathcal{M},\mathcal{W}_{zz}=0$ and $\mathcal{M},\mathcal{W}_{ac}\to\infty$, respectively, indicating the breaking of time-reverse symmetry in both cases. In Fig. 3(c) we show (top to down) Eq. (19) for $\mathcal{W}_{ac}=0.5,\infty(\mathcal{W}_{st}=\mathcal{M}=\mathcal{W}_{zz}=0)$ and Eq. (22) for $\mathcal{M},\mathcal{W}_{zz}=0.5,\infty$ $(\mathcal{W}_{st}=0)$.

D. Correlation function

After analyzing in detail the variance of the conductance of the chaotic Dirac quantum dot from Eq. (19), we briefly study how the correlation function $\mathcal{C}_{\mathcal{F}}(\delta\epsilon,\delta\mathcal{X})$, or covariance of conduction, is affected by straining and boundary parameters. Substituting $\epsilon'=\epsilon+\delta\epsilon$ and $x'=x+\delta x$ in Eq. (19), we can write

$$\frac{\mathcal{C}_{\mathcal{F}}(\delta\epsilon,\delta\mathcal{X})}{G_0^2}=C_\lambda\times\frac{1}{|1+i\delta\epsilon+\delta\mathcal{X}^2|^2},\tag{23}$$

where C_λ is a constant ($\lambda=\{0,\mathcal{X},\mathcal{W}_{st},\mathcal{M},\mathcal{W}_{ac},\mathcal{W}_{zz}\}$), while $C_0=4\times2$, with all parameters set to zero, $C_{\mathcal{X}}=4\times1$ with $\mathcal{X}\to\infty$ and all other parameters set to zero, $C_\lambda=2\times2$ with $\mathcal{M},\mathcal{W}_{ac},\mathcal{W}_{zz}\to\infty$ and the other parameters being zero, and $C_{\mathcal{W}_{st}}=2\times1$ with $\mathcal{W}_{st}\to\infty$ and other parameters set to zero. For $\delta\mathcal{X}=0$, the correlation function is a typical Lorentzian:

$$\frac{\mathcal{C}_{\mathcal{F}}(\delta\epsilon)}{G_0^2}=C_\lambda\times\frac{1}{1+\delta\epsilon^2},$$

which is in accord with the experiment of Ref. [13]. Moreover, for $\delta\epsilon=0$ the correlation function is a quadratic Lorentzian:

$$\frac{\mathcal{C}_{\mathcal{F}}(\delta\mathcal{X})}{G_0^2}=C_\lambda\times\frac{1}{(1+\delta\mathcal{X}^2)^2},$$

which is in agreement with the result of analysis in the experiment of Ref. [12]. Lorentzian and quadratic Lorentzian shapes of the correlation function are plotted in Fig. 4. These findings are encouraging as they confirm the premise of this paper that chaotic Dirac quantum dots containing relativistic electrons obeying the Dirac equation, exhibit universal fluctuations describable by RMT.

V. CONCLUSIONS

In this paper the random nature of the conductance in chaotic Dirac quantum dots is investigated using the RMT-based stub mode. Analytical results for the average conductance and the correlation function are obtained and scrutinized under different limiting stations. The results coincide with those obtained using the semiclassical approach and, when available, agree with experimental findings. Accordingly, the chaotic graphene quantum dot, also called the chaotic Dirac quantum dot, with the electron motion governed by the Dirac equation is a mesoscopic system that follows the rules of RMT, just as the chaotic Schrödinger quantum dot.

Our paper contains several new results of potential use by experimentalists and theorists alike. These include the mechanisms of the breakdown of phase coherence and its impact on the universal fluctuations, and in the quantum interference terms and their effects. We have considered only coupling to ideal leads. Generalization to nonideal leads which effectively modify locally the contact with the quantum dot, is called for. As a result of such generalization, the conductance is modified owing to the influence of special classical trajectories [51]. In our scattering theory approach, this generalization can be handled through the use of nonvanishing tunneling barriers. In the context of scattering theory, such barriers would change the average S matrix, an important ingredient in both the analytical development as well as in the numerical simulations. This line of research is in progress.

ACKNOWLEDGMENT

This work was partially supported by the Brazilian agencies CNPq, FAPESP, CAPES, Instituto Nacional de Ciência e Tecnologia-Informação Quântica/Ministerio de Ciência e Tecnologia, Fundação de Amparo a Ciência e Tecnologia do Estado de Pernambuco, and Centro de Pesquisa, Inovação e Difusão-Optics and Photonic Research Center/FAPESP.

[1] K. S. Novoselov, A. K. Geim, S. V. Morozov, D. Jiang, M. I. Katsnelson, I. V. Grigorieva, S. V. Dubonos, and A. A. Firsov, Nature (London) **438**, 197 (2005).

[2] Y. Zhang, Y.-W. Tan, H. L. Stormer, and P. Kim, Nature (London) **438**, 201 (2005).

[3] A. K. Geim and K. S. Novoselov, Nat. Mater. **6**, 183 (2007).

[4] L. A. Ponomarenko, F. Schedin, M. I. Katsnelson, R. Yang, E. W. Hill, K. S. Novoselov, and A. K. Geim, Science **320**, 356 (2008).

[5] C. W. J. Beenakker, Rev. Mod. Phys. **80**, 1337 (2008).

[6] J. Guttinger, F. Molitor, C. Stampfer, S. Schnez, A. Jacobsen, S. Droscher, T. Ihn, and K. Ensslin, Rep. Prog. Phys. **75**, 126502 (2012).

[7] C. Volk, C. Neumann, S. Kazarski, S. Fringes, S. Engels, F. Haupt, A. Müller, and C. Stampfer, Nature Communications **4**, 1753 (2013).

[8] T. O. Wehling, A. M. Black-Schaffer, and A. V. Balatsky, Adv. Phys. **63**, 1 (2014).

[9] G. Tkachov and E. M. Hankiewicz, Phys. Rev. B **84**, 035444 (2011).

[10] S. V. Morozov, K. S. Novoselov, M. I. Katsnelson, F. Schedin, L. A. Ponomarenko, D. Jiang, and A. K. Geim, Phys. Rev. Lett. **97**, 016801 (2006).

[11] R. V. Gorbachev, F. V. Tikhonenko, A. S. Mayorov, D. W. Horsell, and A. K. Savchenko, Phys. Rev. Lett. **98**, 176805 (2007).

[12] M. B. Lundeberg, R. Yang, J. Renard, and J. A. Folk, Phys. Rev. Lett. **110**, 156601 (2013).

[13] D. W. Horsell, A. K. Savchenkoa, F. V. Tikhonenkoa, K. Kechedzhi, I. V. Lerner, and V. I. Fal'ko, Solid State Commun. **149**, 1041 (2009).

[14] A. Cresti, F. Ortmann, T. Louvet, D. Van Tuan, and S. Roche, Phys. Rev. Lett. **110**, 196601 (2013).

[15] Y.-J. Xiong and B.-K. Xiong, J. Appl. Phys. **109**, 103707 (2011).

[16] E. McCann, K. Kechedzhi, V. I. Fal'ko, H. Suzuura, T. Ando, and B. L. Altshuler, Phys. Rev. Lett. **97**, 146805 (2006).

[17] A. F. Morpurgo and F. Guinea, Phys. Rev. Lett. **97**, 196804 (2006).

[18] J. Wurm, A. Rycerz, I. Adagideli, M. Wimmer, K. Richter, and H. U. Baranger, Phys. Rev. Lett. **102**, 056806 (2009).

[19] K. Wakabayashi, Y. Takane, and M. Sigrist, Phys. Rev. Lett. **99**, 036601 (2007); K. Wakabayashi, Y. Takane, M. Yamamoto, and M. Sigrist, New J. Phys. **11**, 095016 (2009).

[20] E. McCann and V. I. Fal'ko, Phys. Rev. Lett. **108**, 166606 (2012).

[21] I. V. Gornyi, V. Yu. Kachorovskii, A. D. Mirlin, and P. M. Ostrovsky, Phys. Status Solidi B **251**, 1786 (2014).

[22] J. Wurm, K. Richter, and I. Adagideli, Phys. Rev. B **84**, 075468 (2011).

[23] P. Jacquod, R. S. Whitney, J. Meair, and M. Buttiker, Phys. Rev. B **86**, 155118 (2012).

[24] J. Wurm, K. Richter, and I. Adagideli, Phys. Rev. B **84**, 205421 (2011).

[25] R. Yang, L. Huang, Y.-C. Lai, and C. Grebogi, Europhys. Lett. **94**, 40004 (2011).

[26] A. Rycerz, Phys. Rev. B **85**, 245424 (2012); **87**, 195431 (2013); L. Huang *et al.*, Phys. Rev. E **81**, 055203(R) (2010).

[27] M. S. M. Barros, A. J. Nascimento Júnior, A. F. Macedo-Júnior, J. G. G. S. Ramos, and A. L. R. Barbosa, Phys. Rev. B **88**, 245133 (2013).

[28] J. H. Bardarson, M. Titov, and P. W. Brouwer, Phys. Rev. Lett. **102**, 226803 (2009).

[29] F. Libisch, C. Stampfer, and J. Burgdörfer, Phys. Rev. B **79**, 115423 (2009).

[30] M. Wimmer, A. R. Akhmerov, and F. Guinea, Phys. Rev. B **82**, 045409 (2010).

[31] Q. Ma, T. Tu, L. Wang, C. Zhou, Z. Lin, M. Xiao, and G. Guo, Mod. Phys. Lett. B **27**, 1350008 (2013).

[32] D. Subramaniam, F. Libisch, Y. Li, C. Pauly, V. Geringer, R. Reiter, T. Mashoff, M. Liebmann, J. Burgdörfer, C. Busse, T. Michely, R. Mazzarello, M. Pratzer, and M. Morgenstern, Phys. Rev. Lett. **108**, 046801 (2012).

[33] P. G. Silvestrov and K. B. Efetov, Phys. Rev. Lett. **98**, 016802 (2007).

[34] M. Berry and R. Mondragon, Proc. R. Soc. London, Ser. A **412**, 53 (1987).

[35] P. W. Brouwer, J. N. H. J. Cremers, and B. I. Halperin, Phys. Rev. B **65**, 081302(R) (2002).

[36] J. Wurm, M. Wimmer, and K. Richter, Phys. Rev. B **85**, 245418 (2012).

[37] H. Feshbach, Ann. Phys. (NY) **5**, 357 (1958).

[38] H. Feshbach, Ann. Phys. (NY) **19**, 287 (1962).

[39] H. Feshbach, *Theoretical Nuclear Physics: Nuclear Reactions* (Wiley-VCH, Weinheim, 1993).

[40] L. F. Canto and M. S. Hussein, *Scattering Theory of Molecules, Atoms and Nuclei* (World Scientific, Singapore, 2013).

[41] C. Mahaux and H. A. Weidenmüller, *Shell Model Approach to Nuclear Reactions* (North-Holland, Amsterdam, 1969).

[42] J. J. M. Verbaarschot, H. A. Weidenmüller, and M. R. Zirnbauer, Physics Reports **129**, 367 (1985).

[43] G. E. Mitchell, A. Richter, and H. A. Weidenmüller, Rev. Mod. Phys. **82**, 2845 (2010).

[44] B. Dietz, T. Friedrich, H. L. Harney, M. Miski-Oglu, A. Richter, F. Schäfer, and H. A. Weidenmüller, Phys. Rev. E **81**, 036205 (2010).

[45] P. E. Mello and N. Kumar, *Quantum Transport in Mesoscopic Systems: Complexity and Statistical Fluctuations* (Oxford University Press, Oxford, 2004).

[46] See, e.g., J.-H. Cremers, P. W. Brouwer, and V. I. Fal'ko, Phys. Rev. B **68**, 125329 (2003).

[47] P. W. Brouwer, K. M. Frahm, and C. W. J. Beenakker, Waves in Random Media **9**, 91 (1999).

[48] P. W. Brouwer and C. W. J. Beenakker, J. Math. Phys. **37**, 4904 (1997).

[49] G. Wang, L. Ying, and Y.-C. Lai, Phys. Rev. E **92**, 022901 (2015).

[50] D. K. Ferry *et al.*, Semicond. Sci. Technol. **26**, 043001 (2011); R. Brunner *et al.*, J. Phys.: Condens. Matter **24**, 343202 (2012).

[51] R. G. Nazmitdinov, K. N. Pichugin, I. Rotter, and P. Šeba, Phys. Rev. B **66**, 085322 (2002); **66**, 241302 (2002).